18èmes Journées Internationales de Thermique (JITH 2017)
Monastir (Tunisie), 25 - 27 Octobre 2017

Link-Wise Artificial Compressibility Method for simulating thermal convective flows in two dimensions

Hamdi Mohamed[#(1)], Elalimi Souheil[*(2)], Ben Nasrallah Sassi[*(3)]
[#] Laboratory of Wind Power Control and Waste Energy Recovery, Research and Technology Center of Energy, Borj-Cedria,BP95 Hammams Lif 2050,Tunisia.
[*]Energy and Thermal Systems Laboratory, National Engineering School of Monastir, University of Monastir Avenue Ibn El Jazzar, Monastir 5019, Tunisia.

[(1)]***hmdimohamed@gmail.com***, [(2)]*souheil.elalimi@gmail.com*,[(3)]*sassi.bennasrallah@yahoo.fr*

Abstract : Lattice Boltzmann Method (LBM) with recently developed Link-wise artificial compressibility model (LW-ACM) is presented and an application to convective flow is executed. Simulations of thermo-hydrodynamics with the Boussinesq approximation highlighted the robustness, accuracy and efficiency of the proposed methodology. Compared to the multiple-relaxation-time (MRT) implementation, the main advantage of the new formulation is its simplicity and suitability for parallel implementations.

Keywords : Lattice Boltzmann Method (LBM), Artificial compressibility model (ACM), convective flow.

1. Introduction

It is about twenty years ago that the Lattice Boltzmann Method, commonly called LBM, was introduced as a new alternative for the numerical simulation of physical phenomena that can address many problems in physics [1]. Lattice Boltzmann Method sustains today a rapid evolution in terms of physical models, computer implementations and engineering applications. The evolutionary process and the formulation of LBM can be highlighted as the following: The Lattice Gas Cellular Automat (LGCA), the continuous Boltzmann-BGK then the Grad's Hermite-quadrature expansion.Since its development, LBM demonstrated a successful progress not only in solving viscous flow problems [2] but also in heat transfer area [4]. The first connection of the LBE to the Boltzmann equation has been established by He and Luo (1997). These formulations can construct models that recover incompressible Navier-Stokes equations.

The Bhatnagar-Gross-Krook (BGK) approximation [5] is the most popular lattice Boltzmann model. This approach derived from the Enskog equation. In this model the collision operator requires the same relaxation time to each physical quantity. Although it's simple implementation, the BGK-LBM suffers from numerical instability at high Reynolds (or Rayleigh number) number. To avoid this restriction, the direct way is to use a large number of grid points, however this will cost large computer resources and lower the computational efficiency. To remove numerical instability defects of LBM, some authors [4] used the multiple relaxation times model (MRT). The advantage of this model is that it has a maximum number of adjustable parameters. These parameters can be determined by optimizing the hydrodynamic properties of the model and linear stability analysis of the LBE evolution operator. Another way to remedy the stability problem in LBM, is to return into the definition of entropic definition of LBM. Some authors who refer to each other [6] used entropic lattice Boltzmann schemes. The derivation of ELBE can be performed in many ways and the most popular one derived from the analog of the discrete Boltzmann H function of standard extensive statistical mechanics [7].

The artificial compressibility method (ACM) introduced by Chorin in 1967 [8] to solve the incompressible Navier–Stokes equations (INSE) is recently developed with an easy formulation known as Link Wise Artificial Compressibility Method that benefits from some similarities between its classic formulation and Lattice Boltzmann Methods (LBM) [9]. Asinari et al. [10] developed the LW-ACM by a finite set of discrete directions (links) on a regular lattice mesh similar to LBM and demonstrated the stability and accuracy of the proposed model. It should be mentioned that the link between LBM and ACM was observed earlier by He et al.

[11] and they performed a comparison between the two methods. Their results showed that LBM and ACM are closely related to each other. The similarities between them appears in the continuous form of macroscopic governing equations while they differ from each other in their discrete forms. Also they found that difference between LBM and ACM do not affect the momentum results but it has an impact on the pressure fields. Obrecht and Kuznik [12] used an hybrid thermal LW-ACM to solve differentially heated cubic cavity. Their results showed that this scheme remains stable until Rayleigh number $Ra = 10^8$. In fact, LW-ACM can be used with double-population model and simulate convective flows [13] and save the Memory usage compared to MRT-LBM. Obrecht et al. [14] performed for a comparison between LW-ACM and LBM using lid-driven cubic cavity flow problem. The obtained results showed that LW-ACM is more accurate than multiple-relaxation-time LBM .

2. LW-ACM for dynamic and thermal fields

The incompressible Navier-Stokes equations are in the following form.

$$\nabla . u = 0 \tag{1}$$

$$\partial_t u + Re \times u . \nabla . u = -\nabla p + \nabla^2 u \tag{2}$$

The introduction of an artificial compressibility δ into the equation of motion do not affect the results and acts in the manner as the relaxation parameter in LBM. The ACM substitutes the equation of conservation of mass into the artificial compressibility equation (ACE) .

$$\delta \times \partial_t p + \nabla . u = 0 \tag{3}$$

The artificial density can be determined easily by using the equation of state $p = \rho/\delta$. This yields an artificial speed of sound $c_s = 1/\sqrt{\delta}$. The explicit time-marching and working on regular Cartesian grid make some analogies between ACM and LBM .

In LBM the particle distributions defined for the finite set of the discrete particle velocity vectors c_i at a site r at time t is denoted $f_i(r,t), i = 0..8$. In two dimension, the direction of a single particle probability distribution function is limited to nine directions as follows:

$$c_i = \begin{cases} (0,0) & i = 0, \\ (\pm 1, 0) & i = 1-4, \\ (\pm 1, \pm 1) & i = 5-8. \end{cases} \tag{4}$$

The link-wise artificial compressibility method (LW-ACM) is recently developed in the same manner as LBM models starting from the ACM and using analog integration strategy. In this model the dynamic behaviour of the fluid is described by the evolution process of the distribution function in discrete velocity can be written as:

$$f_i(r + c_i\delta_t, t + \delta_t) - f_i(r,t) = 2\left(\frac{1-\tau}{\tau}\right)\left(f_i^{eq,o}(r + c_i\delta_t, t + \delta_t) - f_i^{eq,o}(r,t)\right) \tag{5}$$

$$f_i^{eq,o}(\rho, u) = \frac{1}{2}\left(f_i^{eq}(\rho, u) - f_i^{eq}(\rho, -u)\right) \tag{6}$$

τ is the relaxation time and $f_i^{eq,o}$ is the local equilibrium distribution function that has an appropriately prescribed functional dependence on the local hydrodynamic properties as follows:

$$f_i^{eq,o}(\rho, u) = \omega_i \rho \left[1 + 3u . c_i + \frac{9}{2}(u . c_i)^2 - \frac{3}{2}u^2\right] \tag{7}$$

The weights ω_i are given by : $\omega_0 = \frac{4}{9}$, $\omega_{1-4} = \frac{1}{9}$ and $\omega_{5-6} = \frac{1}{36}$.

τ is the relaxation time given by :

$$\tau = \frac{1}{2} + \frac{3\nu}{c^2 \Delta t} \tag{8}$$

c_s is the speed of sound. The pressure and the flow velocity in lattice unit are obtained through moment summations in the velocity space as follows:

$$p = \frac{1}{3}\sum_i f_i(r,t), \; u = \frac{\sum_i c_i f_i(r,t)}{\sum_i f_i(r,t)} \tag{9}$$

The conversion from lattice to physical units can be easily computed from the following equations:

$$p_{ph} = (p - p_0)/\epsilon^2, \; u_{ph} = u/\epsilon, \quad \epsilon = 1/N \tag{10}$$

N the number of mesh points along the characteristic length of the problem.
To solve advection-diffusion equation for the temperature, we use D2Q5 model. We consider only five discrete velocities $c_i = \{1,..5\}$. the thermal evolution equation can be written as the following:

$$g_i(r + c_i\delta_t, t + \delta_t) - g_i(r,t) = 2\left(\frac{1-\tau}{\tau}\right)\left(g_i^{eq,o}(r + c_i\delta_t, t + \delta_t) - g_i^{eq,o}(r,t)\right) \quad (11)$$

$$g_i^{eq,o}(T,u) = \frac{1}{2}\left(g_i^{eq}(T,u) - g_i^{eq}(T,-u)\right) \quad (12)$$

Where

$$g_i^{eq}(T,u) = \omega_i T\left[1 + 3u.c_i + \frac{9}{2}(u.c_i)^2 - \frac{3}{2}u^2\right] \quad (13)$$

The temperature in LBM unit is computing by conserving only the first moment:

$$T = \sum_i g_i(r,t) \quad (14)$$

The relations between the diffusion coefficient and the relaxation time are taken as below:

$$\tau_t = \frac{1}{2} + \frac{3\left(\frac{\kappa}{\rho C_p}\right)}{c^2\Delta t} \quad (15)$$

κ ρ and C_p are the thermal conductivity, density and the specific heat capacity of the fluid. The introduction of the force term can be done in various ways. It consists of changing the equilibrium distribution functions by applying the contribution of the force in each direction. The body force F gives rise to a buoyancy force F, and is defined from equation (6) such that.

$$F = 3\omega_i\frac{c_i F}{c^2}; \quad \mathbf{F} = \rho_0\beta(T - T_0)\mathbf{g} \quad (16)$$

β is the thermal expansion coefficient of fluid and g is the gravity. With this formulation, the model solves the following energy equation:

$$\partial_t T + (u\nabla)T = \left(\frac{\kappa}{\rho C_p}\right)\nabla^2 T \quad (17)$$

For computer implementation, the algorithm of the double population LW-ACM looks as follows:

(i) Initialisation of ρ_0, T_0, u_0 and the distribution functions $f_i^{eq,o}(\rho_0, u_0), g_i^{eq,o}(\rho_0, T_0)$.
(ii) Advection of f_i and g_i.
(iii) Compute the equilibrium function $f_i^{eq,o}(\rho,u)$ and $g_i^{eq,o}(\rho,T)$ using Eq.(4) .
(iv) Apply the boundary conditions.
(v) Compute conserved quantities ρ, T and u.
(vi) If t reaches the specified convergence condition, then the computation is terminated.
(vii) Otherwise, processes (ii)-(v) are repeated.

2. Numerical experiments

2.1. LW-ACM versus other LB models

As it has been developed in section 1, there are several methods used to enhance LBM stability and accuracy. The LW-ACM is a new strategy in this issue. Some important points have to be discussed and analyzed before performing simulations using this model, such as: its efficiency in terms of rapidity and accuracy against BGK which is the most widely used model and MRT which is the most stable and accurate model [4]. We consider the classical 2-D natural convection in a square cavity heated differentially on the vertical side walls. This problem has been extensively employed as a standard benchmark for numerical methods and has been analyzed by a number of authors using a variety of solution procedures.
The characteristic velocity in the buoyant flow $U^b = \sqrt{g\beta\Delta TH}$ is taken so that Mach number is within the incompressible limit and small compared with the speed of sound (Ma<<1). At all walls, bounce-back boundary conditions were applied. In this case, the incoming distribution functions turned back to the site where they are from. For thermal boundary conditions, two types of boundary conditions are used. One is the isothermal boundaries and the other is the adiabatic boundaries. For isothermal boundaries (Dirichlet type boundary condition) the normal equilibrium condition [15] was used to determine the unknown densities. Results are assumed to be converged when we reach the following convergence criterion.

$$\frac{\Sigma_{i,j}\|u((i,j),t+1)-u((i,j),t)\|_2}{\Sigma_{i,j}\|u((i,j),t)\|_2} < 10^{-8} \quad (18)$$

$$\max\left(\left|T\left((i,j),t+1\right)-T\left((i,j),t\right)\right|\right) < 10^{-6} \quad (19)$$

The non-dimensionalized heat transfer at the isothermal walls is represented by the Nusselt number:

$$Nu = \int_0^1 \frac{\partial\theta}{\partial X}\Big|_{X=0} dY \simeq \sum_1^M \frac{3\theta(0,j)-4\theta(1,j)+\theta(2,j)}{2} \quad (20)$$

Where θ is the adimensionalized temperature and M is the number of nodes in the y direction.

The MRT-LBM code is validated for a two-dimensional simulation of Raiylegh-Bénard convection at different Rayleigh numbers was performed with a Prandtl number of 0.71 (air). The critical Rayleigh number for the onset of the Rayleigh-Benard convection is 1707.74 which agrees with the theoretical prediction [16]. As the Rayleigh number is increased higher, the steady two-dimensional convection rolls become unstable. The wavy instability and periodic motion observed are in good agreement with experimental observations and theoretical predictions. At the first levels of the simulation, the generation of the mushroom-like isotherms (plumes) is observed. It is caused by the instability and the instantaneous thickness in the conduction layer. This phenomenon can be observed in turbulent convection at high Rayleigh number [17]. The isotherms show a higher level of convective activity and a thin thermal boundary layers. The boundary layer become more thinner compared to results of the convective flow with Pr=0.71. It is important to mention here that similar results of Snapshot contour plots are found experimentally by Sparrow [18] using electrically heated horizontal copper surfaces situated in a water medium. They used electrochemica1 technique to facilitate physical observations. In particular, the transient state isotherms obtained at the beginning of the calculation with the MRT-LBM code reproduce the mushroom-like appearance as observed by in [18].

Another validation of the MRT-LBM code, is the resolution of the mixed convection heat transfer of fluid over microscale vertical duct preceded with a double-step expansion. The fluid is injected into the channel at a cooler temperature T_0 and with a fully developed velocity profile. Channel expansion ratio, $A = L/h$, is taken equal to 30 and the overall length of the computational domain is $L = 35h$. The centerline velocity at the inlet and the fluid viscosity is taken so that Mach number is within the limit of incompressible flow. Thus, the magnitude velocity for both the buoyant and forced flows are taken small compared with the speed of sound (Ma<<1). The walls downstream of the step are maintained at a constant temperature T_1, while the other walls are treated adiabatically. The results for mixed convection flow with air (Pr=0.71) have been compared with numerical results reported in [19] using finite-volume method. Computations were performed with 702×62 grid size. Velocity profiles at the particular axial position Y=5 for fixed Reynolds number Re=114 and for the Grashof number ranging from $Gr = 10^2$ to $Gr = 10^4$ has been compared with those obtained by Tsui and Shu [19] in Figure 1. It is shown that numerical results of the MRT model compares well with the numerical data.

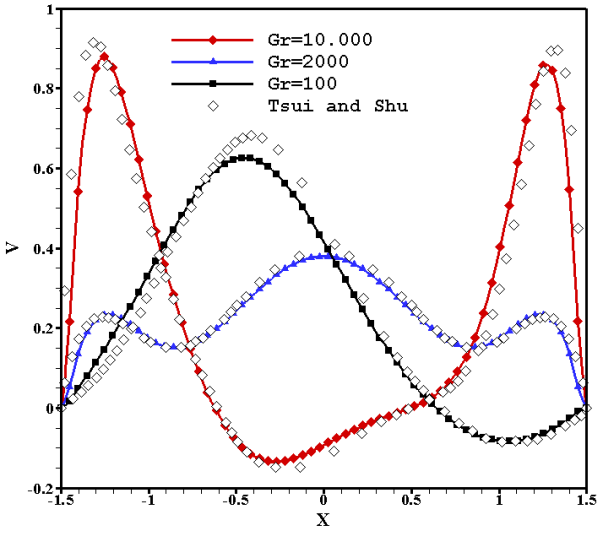

Figure 1 : Velocity profiles at X = 5 and Re = 114 (Pr=0.71).

In Table 1, we show computed Nusselt numbers and Processor time required with different models for *Pr*=0,71 and Ma=0,05 obtained by the BGK, MRT and LW-ACM method for Rayleigh number from 10^3 to 10^5.

As it can be seen from all chosen Rayleigh numbers, the LW-ACM model gives results closer to the reference [20] than the BGK model. As it was expected, MRT simulation gives analogous results as those reported in the reference even we use a coarse mesh. The table provides the CPU time required to attain the steady state according to the prescribed criterion of the BGK, MRT, and LW-ACM schemes. Clearly, we can see that the CPU time for BGK model is the shortest. It is true that MRT model is more accurate, but it requires more time to reach steady state. The results also show that, the MRT scheme is about 23% and 12% slower than the BGK scheme in terms of CPU time.

Table1 : Computed Nusselt numbers and Processor time required with different models for Pr=0,71 and Ma=0,05.

Ra	Grid size	Wang et al. (2013)	BGK	Δ %	CPU	MRT	Δ %	CPU	LW-ACM	Δ %	CPU
10^3	64^2	1,1178	1,1170	0,071	30,11	1,1174	0,035	40,11	1,1173	0,044	44,65
	128^2		1,1171	0,062	63,31	1,1175	0,026	78,01	1,1174	0,035	70,23
	256^2		1,1172	0,053	81,22	1,1178	0,0	110,22	1,1178	0,0	95,368
10^4	64^2	2,2448	2,2430	0,080	45,21	2,2445	0,013	54,26	2,2443	0,022	48,05
	128^2		2,2436	0,053	76,02	2,2443	0,022	91,01	2,2440	0,035	85,67
	256^2		2,2444	0,017	140,21	2,2446	0,008	180,41	2,2444	0,017	156,51
10^5	64^2	4,5216	4,5172	0,097	65,25	4,5185	0,068	80,21	4,5180	0,079	72,38
	128^2		4,5185	0,068	150,21	4,5195	0,046	198,25	4,5193	0,050	171,32
	256^2		4,5110	0,013	320,00	4,5202	0,030	400,25	4,5200	0,035	361,49

In order to validate the LW-ACM code, the results for natural convection flow in a square cavity in which the fluid is heated from below and cooled from above have been compared with numerical results reported in the literature using finite-volume method. Average Nusselt number for Rayleigh number ranging from 10^3 to 10^5 has been compared with those obtained by Clever and Busse [21] in Figure 2. It is shown that our numerical results compares well with the numerical and empirical data based on the formula $Nu = 1.56(Ra/Ra_c)^{0.296}$.

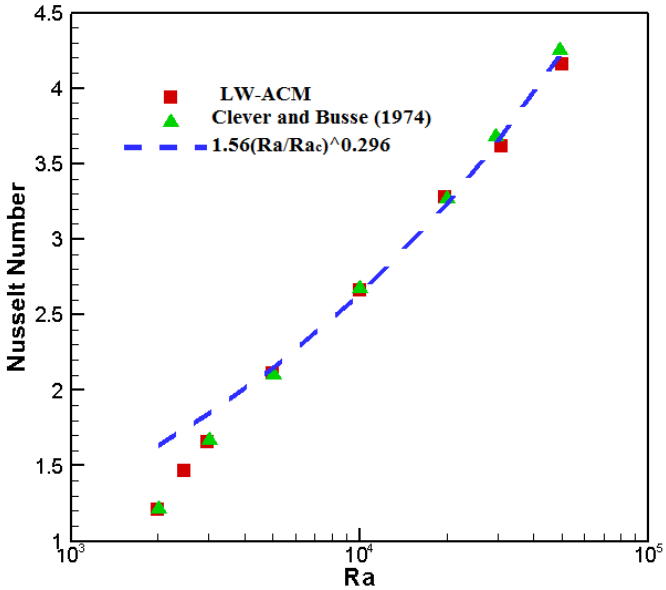

Figure 2 : Variation of Nusselt number for 2D Rayleigh-Bénard problem with Rayleigh number for Pr=0.71.

2.2. Magnetic field effects on free convection

To test the double population LW-ACM ability to solve more complex flows, we perform numerical study of the magnetoconvection in a square cavity. Recently, This problem sustains a considerable attention because of a number of its wide variety of applications in engineering and technology such as metallic alloy, magnetoelectrochemistry (MEC), astrophysical and environmental systems [22, 23]. Thus, it has been shown both experimentally and numerically that magnetic fields can be used to control thermal convection which is

important from problem involving the metallurgy, microstructure devices, protein crystals and under reduced gravity conditions .

In order to evaluate the potential effects of magnetic fields in heat transfer area, some studies appears in recent years. Benos et al. [24] solved analytically and numerically two-dimensional MHD natural convection flow in an internally heated horizontal shallow cavity. Their comparison of the analytical and numerical results showed the validity and the correctness of their analysis. It is of interest to note that the recent progress in superconductivity and electric resistance of metals at very low temperature allowed researchers to reach larger magnetic fields up to 15 T by using super-conducting magnets. Naffouti et al. [25] performed numerical study of Rayleigh-Bénard magnetoconvection for different Rayleigh number, Hartmann number and inclination angle of magnetic field. Their results showed a decrease in heat transfer with the increase of both the Hartmann and Rayleigh numbers. Effects of strong magnetic field on two dimensionnal natural convection have been studied by Pirmohammadi and Ghassemi [26]. They found that when Hartmann number is sufficiently large, the convection is suppressed. Bouabdallah and Bessaïh [27] conducted experimental and numerical study to present magnetic field effect on fluid flow and heat transfer during solidification from a melt. Their results showed a strong dependence between the solid/liquid interface shape, the intensity and the orientation of magnetic field. Gajbhiye and Eswaran [28] studied numerically the effect of an imposed magnetic field on Rayleigh-Bénard convection in constricted 2-D geometry. Their results showed that the flow solution abruptly turns from steady state to oscillatory flow as the Rayleigh number increases from $Ra=8.10^3$ to $Ra=10^4$. Ahmed et al. [29] performed numerical study of laminar magneto hydrodynamic mixed convection in an inclined lid-driven square cavity with opposing temperature gradients. Their results indicate that the rate of heat transfer along the heated walls is enhanced on increasing either Hartmann number or inclination angle. Average Nusselt number also, increased with increasing of the amplitude ratio for all values of the phase deviation. Nasrin and Alim [30] used the Galerkin weighted residual control volume finite element method to perform the effects of magnetic field and Joule heating on combined convection flow and heat transfer characteristics inside an octagonal vertical channel containing a heat-generating hollow circular pipe at the centre. Their results showed that that the flow and thermal fields in the vertical channel depend markedly on the Hartmann, Richardson and Joule heating parameter. Kahveci and Öztuna [31] investigated the MHD flow and heat transfer in a tilted enclosure with a centered partition and found that for high Rayleigh numbers, the average Nusselt number shows an increasing trend as the inclination angle increases and a peak value is detected. Beyond the peak point, the trend reverses to decrease with further increases in the inclination angle. Ozoe and Okada [32] studied numerically three-dimensional magneto convection with sample Prandlt number Pr=0.054 and two Rayleigh number 10^6 and 10^7. They found that external magnetic field perpendicular to the vertical boundary layer type flow is the most effective in cancelling the convective flow. However, the vertical component of magnetic field is not effective.

In spite of the existence of many papers dealing with the interaction between convection and magnetic fields, there is as yet no complete understanding of magnetoconvection and further research works still needed to provide certain important feature. In this work, the cavity is filled with an electrically conducting, viscous and incompressible fluid with negligible viscous dissipation and radiation effects and a uniform and horizontal magnetic field B is applied. We assume that chemical reaction is negligible. The continuity (1), the extended momentum (2) and the energy equations (3) for natural convection flow under Boussinesq approximation can be written as follows:

$$\nabla u = 0 \tag{21}$$

$$\partial_t u + (u\nabla)u = -\frac{1}{\rho}\nabla p + \nu\nabla^2 u + f^b + f^m \tag{22}$$

$$\partial_t T + (u\nabla)T = \left(\frac{\kappa}{\rho C_p}\right)\nabla^2 T \tag{23}$$

f^b is the buoyancy force and f^m is the magnetic force due to the presence of magnetic field defined as:

$$f^m = \frac{1}{\rho} J \times B \tag{24}$$

Where $J = \sigma(-\nabla\phi + u \times B)$ is the current density obtained by using Ohm's Law, ϕ is the electric potential.

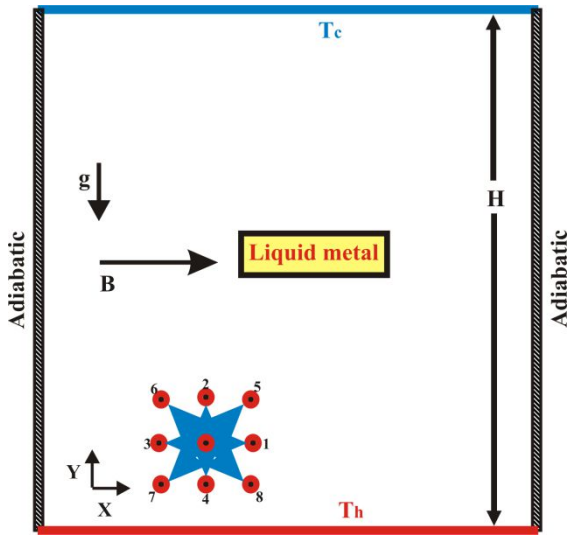

Figure 3 : Illustration of the flow and boundary conditions of the problem.

In the literature, the effects of magnetic fields on the steady flow at relatively low Rayleigh number have been thoroughly investigated [33]. However, their effects on transient flow at high Rayleigh number ($Ra > 10^6$) remains to be insufficiently understood and make the object of the present investigation.
The effect of magnetic fields on natural convection flows for high Rayleigh number $Ra = 10^8$ and Prandtl number of 0.054 is studied. Figure 5 Shows streamlines and steady state isotherms at Rayleigh number $Ra = 5 \times 10^4$ for different Hartmann number (Ha=0, 20, 40 and 60). For all chosen Rayleigh number, an adjustment in the flow pattern is observed when magnetic fields are applied. The rotational flow with a single elliptic vortex is observed for high Hartmann number. Isotherms become more uniformly spaced throughout the cavity and the intensity of convection is considerably decreased by the drag induced by the magnetic field, as indicated by a weak distortion of the isothermal lines.

The magnetic field reduce the Nusselt number and the fluid velocity. When Hartmann number is sufficiently large, the mushroom-like isotherms (plumes) caused by the instability and the instantaneous thickness in the conduction layer become more thinner. Without magnetic fields, the streamlines form two symmetrical vortex which keep the center of the cavity and when magnetic is applied with sufficient value of Hartmann number, the two vortex move from the center of the cavity to the top. The bifurcation of the flow take place for all cases. The two large vortices appear on the center of the enclosure, but with increasing in Hartmann number, the two vortex are reduced in size located near the top and bottom of the right horizontal top wall. The core of vortex depends on the magnitude of magnetic field. Also, the increase in the value of the magnetic field moves the vortex into the top wall where the temperature is cold. We note also a change in the shape of vortices from the circular shape to elliptical one.

One of the application of such result is in melting processes of an electrically conducting fluid metals when the fluid motion presents turbulent convection flow. The applied magnetic field leads to stabilize or cancel unwanted oscillations in the flow. Figure 7 present the evolution of the averaged Nusselt number for different Hartmann numbers. The Nusselt number keep decreasing with respect of Hartmann number, we can highlight that when Ha=60, the effect of magnetic fields on the Nusselt number (and so on the heat transferred through the walls) is significant.

Table 2 summarizes the averaged and overall Nusselt number along the hot wall versus Hartmann numbers. We observe that, in agreement with what has been concluded from thermal and flow fields in Figure 4, Nusselt numbers decrease with the increase of the Ha which has effect of suppressing the convection.

Table 2 : Computed Average Nusselt number for different magnetic field magnitude.

Ha	0	20	40	60
Average Nusselt number	4,261	4,185	2,850	2,768

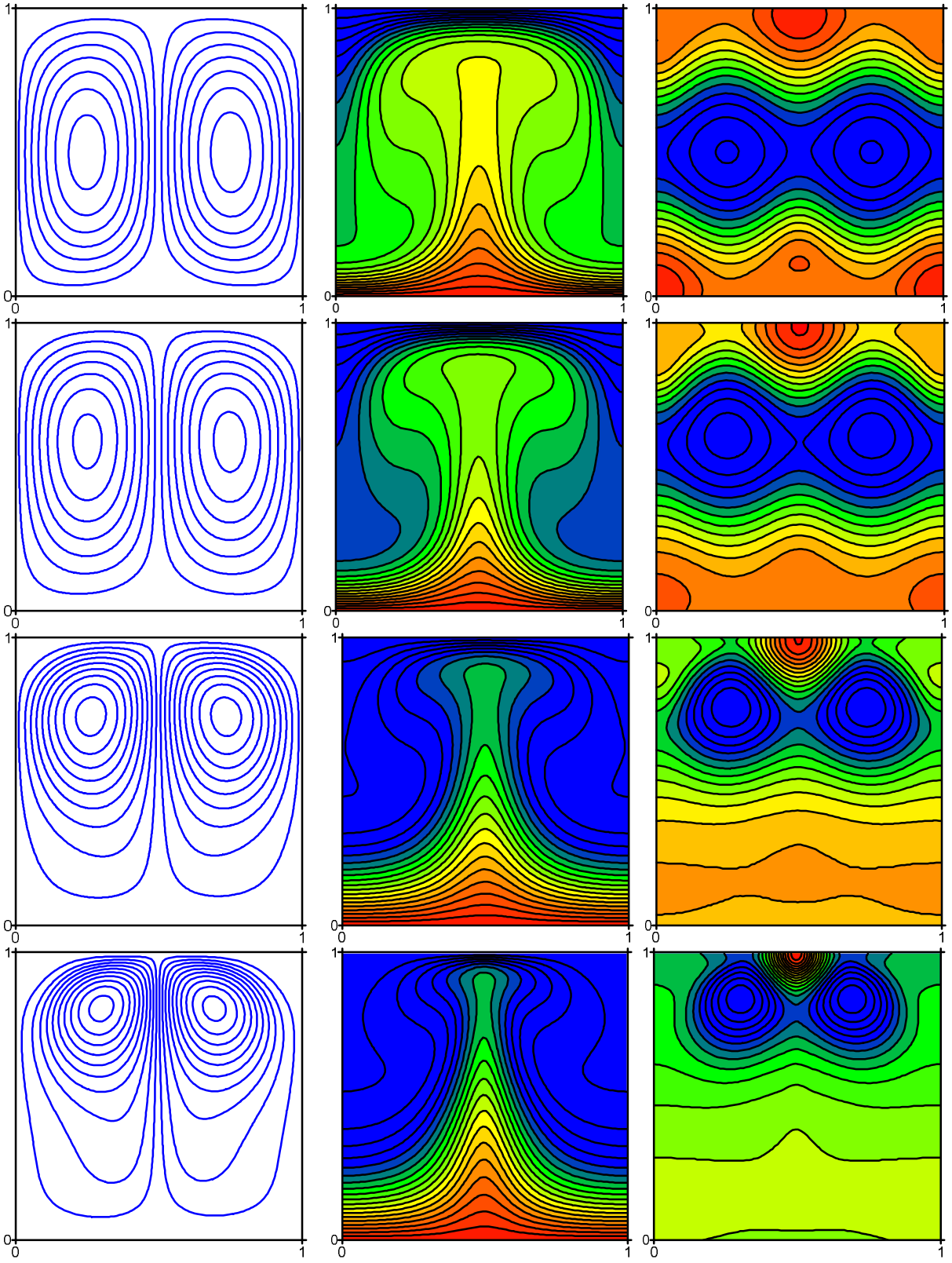

Figure 4 : Streamlines, steady state isotherms and pressure contours (from left to right) at *Ra*=50.000 for *Ha*=0-60 (from top to down).

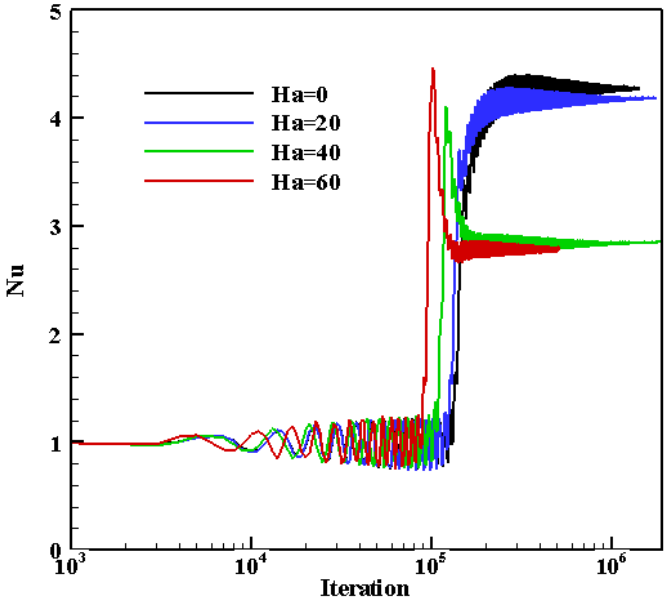

Figure 5 : Convergence of the average Nusselt number with different Hartmann number at *Ra*=50.000.

Conclusion

In this work, a double population Link-Wise Artificial Compressibility Method (LW-ACM) has been developed to solve convective flows. Results of natural convection flows in a square cavity were compared and validated with those using BGK-LBM and MRT-LBM models and the accuracy of the prescribed model was evaluated. This trend demonstrates the robustness and the accuracy of the numerical method for engineering applications.

Nomenclature

Symbols

g Gravitational acceleration.
Ra Rayleigh number $Ra = g\beta\Delta TH^3/\nu\alpha$.
H cavity height.
f_i particle distribution function.
f_i^{eq} equilibrium distribution function for f_i.
$f_i^{eq,o}$ modified equilibrium distribution function for f_i.
g_i energy distribution function.
g_i^{eq} equilibrium distribution function for g_i.
$g_i^{eq,o}$ modified equilibrium distribution function for g_i.
Ma Mach number in the simulation $Ma = u/c_s$.
Nx grid size in x direction, respectively.
Nu local and average Nusselt number.
Ha Hartmann number $Ha = BH\sqrt{\sigma/\mu}$.

Greek symbols

$\Delta x, \Delta y$ regular steps.
ΔT difference in temperature between the plates and the inlet fluid.
$\alpha = k/\rho C_p$ thermal diffusivity, $m^2.s^{-1}$.
β coefficient of thermal expansion of the fluid, K^{-1}.
ρ_0 fluid density in lattice unit.
θ dimensionless temperature.
δ_t time step.

Subscripts

eq equilibrium.
bc boundary condition.
eq, o local equilibrium distribution function.

References

[1] A. A. Mohamad, Applied Lattice Boltzmann Method for Transport Phenomena, Momentum', *Heat and Mass Transfer, Calgary*, 2007.
[2] Chen and Doolen, 1998
[3] A. Mezrhab, M.A. Moussaoui, M. Jami, , H. Naji et M. Bouzidi, Double MRT thermal lattice Boltzmann method for simulating convective flows. *Physics Letters A*, Volume 374, Pages 3499-3507, 2010.

[4] L.S. Luo, W. Liao, X. Chen, Y. Peng et W. Zhang, Numerics of the lattice Boltzmann method: Effects of collision models on the lattice Boltzmann simulations, *Phys. Rev. E*, Volume 83, 056710, Pages 1-24, 2011.
[5] P. L. Bhatnagar, E. P. Gross et M. Krook, A model for collision processes in gases. I. Small amplitude processes in charged and neutral one-component systems', *Phys. Rev.,* Volume 94, Pages 511-525, 1954.
[6] S. Ansumali et I.V. Karlin, Entropy Function Approach to the Lattice Boltzmann Method', *Journal of Statistical Physics*, Volume 107, No.1, Pages 291-308, 2002.
[7] S. Ansumali, I.V. Karlin et H.C. Öttinger, Minimal entropic kinetic models for hydrodynamics, *Europhysics Letters*, Volume 63, No.6, Pages 798-804, 2003.
[8] A. J. Chorin, A numerical method for solving incompressible viscous flow problems, *Journal of Computational Physics,* Volume 2 (1), Pages 12-26, 1967.
[9] T. Ohwada, P. Asinari et D. Yabusaki, Artificial compressibility method and lattice Boltzmann method: Similarities and differences, *Computers and Mathematics with Applications* , Volume 61 (12), Pages 3461-3474, 2011.
[10] P. Asinari, T. Ohwada, E. Chiavazzo et A. Di Rienzo, Link-wise artificial compressibility method, *Journal of Computational Physics*, Volume 231, Pages 5109-5143, 2012.
[10] He et al. (2002)
[11] X. He et L.S. Luo, Lattice Boltzmann Model for the Incompressible Navier-Stokes Equation, *Journal of Statistical Physics*, Volume 88, Pages 927-944, 1997.
[12] C. Obrecht et F. Kuznik, Hybrid thermal link-wise artificial compressibility method. *Physics Letters A*,Volume 379, Pages 2224-2229, 2015.
[13] C. Obrecht, P. Asinari, F. Kuznik and J. J. Roux, Thermal link-wise artificial compressibility method: GPU implementation and validation of a double-population model. *Computers and Mathematics with Applications*, Volume 72 (2), Pages 375-385, 2016.
[14] C. Obrecht, A. Pietro, F. Kuznik et J. J. Roux, High-performance implementations and large-scale validation of the link-wise artificial compressibility method, *Journal of Computational Physics*, Volume 275 (15), Pages 143-153, 2014.
[15] Q. Zou et X. He, On pressure and velocity boundary conditions for the lattice Botlzmann BGK model, *Physics of Fluids*, Volume 9, Pages 1591-1598, 1997.
[16] Reid W.H., D.L. Harris, Some further results on the Bénard problem, *Phys. Fluids* , Volume 1 (2), Pages 102-110, 1958.
[17] J. J. Niemela, L. Skrbek, K. R. Sreenivasan and R. J. Donnelly, Turbulent convection at very high Rayleigh numbers, *Nature*, Volume 404, Pages 837-840, 2000.
[18] E. M. Sparrow, R. B.Husar et R. J. Goldstein, Observations and other characteristics of thermals, *J. Fluid Mech.,* Volume 41(4), Pages 793-800, 1970.
[19] Y.Y. Tsui et S.J. Shu, Effects of buoyancy and orientation on the flow in a duct preceded with a double step expansion, Int. J. Heat and Mass Transfer, Volume 41 (17), Pages 2687-2695, 1998.
[20] J. Wang, D. Wang, P. Lallemand P., Li-Shi Luo, Lattice Boltzmann simulations of thermal convective flows in two dimensions,*Computers and Mathematics with Applications*, Volume 65, Pages262-286, 2013.
[21] R.M. Clever, F.H. Busse, Transition to time-dependent convection, *J. Fluid Mech*., Volume 65 Pages 625-645, 1974.
[22] J.M. Borrero, S. Jafarzadeh, M. Schüssler et S. K. Solanki, Solar Magnetoconvection and Small-Scale Dynamo Recent Developments in Observation and Simulation, *Space Science Reviews*, Springer, in press, 2015.
[23] N. Bekki et H. Moriguchi, Temporal chaos in Boussinesq magnetoconvection, *Physics of Plasmas*, Volume 14, Pages 012306-1-8, 2007.
[24] L. T. Benos, S. C. Kakarantzas, I. E. Sarris, A. P. Grecos et N. S. Vlachos, Analytical and numerical study of MHD natural convection in a horizontal shallow cavity with heat generation, *International Journal of Heat and Mass Transfer* , Volume 75, Pages 19-30, 2014.
[25] A. Naffouti, B. Ben-Beya et T. Lili, Three-dimensional Rayleigh-Bénard magnetoconvection: Effect of the direction of themagnetic field on heat transfer and flow patterns, *C. R. Mecanique*, Volume 342, Pages 714-725, 2014.
[26] M. Pirmohammadi et M. Ghassemi, Effect of magnetic field on convection heat transfer inside a tilted square enclosure, *International Communications in Heat and Mass Transfer*, Volume 36, Pages 776-780, 2009.
[27] S. Bouabdallah et R. Bessaïh, Effect of magnetic field on 3D flow and heat transfer during solidification from a melt, *International Journal of Heat and Fluid Flow*, Volume 37, Pages 154-166, 2012.
[28] N. L. Gajbhiye et Eswaran, V., Numerical simulation of MHD flow and heat transfer in a rectangular and smoothly constricted enclosure. *Int. J. Heat. Mass. Transfer*, Volume 83, Pages 441-449, 2015.
[29] S. E. Ahmed, M. A. Mansour et A. Mahdy, MHD mixed convection in an inclined liddriven cavity with opposing thermal buoyancy force: Effect of non-uniform heating on both side walls, Nuclear Engineering and Design. *Nuclear Engineering and Design*, Volume 265, Pages 938-948, 2013.

[30] R. Nasrin et M., A. Alim, Control volume finite element simulation of MHD forced and natural convection in a vertical channel with a heat-generating pipe, *International Journal of Heat and Mass Transfer*, Volume 55, Pages 2813-2821, 2012.
[31] K. Kahveci et S. Öztuna, A differential quadrature solution of MHD natural convection in an inclined enclosure with a partition, *ASME Journal of Fluids Engineering*, Volume 130, 021102, 2008.
[32] H. Ozoe et K. Okada, The effect of the direction of the external magnetic field on the three-dimensional natural convection in a cubical enclosure, *Int. J. Heat Mass Transfer*, Volume 32, Pages 1939-1954, 1989.
[33] H. F Oztop, M. Oztop et Y. Varol, Numerical simulation of magnetohydrodynamic buoyancy-induced flow in a non-isothermally heated square enclosure, *Communications in Nonlinear Science and Numerical Simulation*, Volume 14, Pages 770-778, 2009.